Time-Averaged and Unsteady Imaging Analysis of a Reacting Fuel Jet in Vitiated Cross-Flow at Elevated Pressure

Ryan Sullivan[1], Benjamin Wilde[1], David R. Noble[2],Karthik Periagaram[1], Jerry M. Seitzman[3],Tim C.Lieuwen[3]
School of Aerospace Engineering, 270 Ferst Drive, Atlanta, GA 30332, USA

This paper describes an experimental imaging and analysis study of a reacting $CH_4/H_2/CO$ jet in a vitiated crossflow. We present an extensive data set showing the variation of the time averaged and unsteady characteristics of the reacting jet over the momentum flux ratio range of $0.75<J<240$. These results show that the reaction initiates on the lee side of the jet and stands off vertically from the injector. The ratio of this standoff distance to jet exit velocity is of the same order of magnitude as the calculated ignition delay of a nonpremixed flame at the "most reactive" mixture fraction. In the nearfield, the time averaged trajectory of the reacting jet is quite close to the Holdeman temperature centerline for nonreacting jets. In the far-field region, the jet penetration into the crossflow exceeded the nonreacting trajectory correlation, presumably due to gas expansion effects from heat release. Analysis of the unsteady jet motions showed that the reacting jet flaps in a sinuous manner with an amplitude that increases with downstream distance. For lower J jets, $J<\sim20$, an intermittent jet attachment effect was observed, where the flame attaches to the wall for some fraction of time that decreases with downstream distance and increasing J.

Nomenclature

$D(x)$	=	Duty cycle
f	=	Frequency
J	=	Jet-to-crossflow momentum flux ratio
P	=	Pressure
Re_d	=	Jet Reynolds Number
T	=	Temperature
St	=	Strouhal number based on jet diameter
Z	=	Mixture fraction
Z_{MR}	=	Most reactive mixture fraction
d	=	Nozzle diameter
u_j	=	Jet velocity
u_m	=	Crossflow velocity
t	=	Time
x	=	Axial position
z	=	Vertical position
z_{ign}	=	Vertical flame standoff location
$\zeta_L(x,t)$	=	Leeward edge position
$\zeta_W(x,t)$	=	Windward edge position
ρ_j	=	Jet density
ρ_m	=	Crossflow denity
τ_1	=	Measured ignition time

[1] Graduate Research Assistant, Ben T. Zinn Combustion Laboratory
[2] Research Engineer II, Ben T. Zinn Combustion Laboratory, AIAA Member
[3] Professor, AIAA Associate Fellow

τ_2 = Calculated ignition time

I. Introduction

THIS paper describes imaging studies of the time averaged and fluctuating characteristics of a turbulent reacting fuel jet in a vitiated crossflow. Jets in crossflow (JICF), or transverse jets, are an important problem for a variety of combustion applications, including fuel/air mixers, flares, quench devices in rich-quench-lean (RQL) combustors, and fluidic flame stabilization[1-5]. The specific reacting JICF problem focused on here appears in a variety of combustion applications where either fuel is injected into an oxidizing stream, such as in a fuel injector or flare [6-9], or air is injected into a fuel-containing stream, such as in the quench section of an RQL combustor [2, 10-14].

More generally, nonreacting and reacting jets in crossflow find application in systems where rapid mixing is required. They entrain and mix ambient fluid at a higher rate [15-17] than other commonly used flow configurations, such as mixing layers and axial jets. The flow field is highly unsteady and three-dimensional, consisting of several coherent vortical structures, namely, the counter-rotating vortex pair (CRVP), the horseshoe vortex system associated with the separating approach flow boundary layer, the jet shear-layer vortices (SLV) and the wake vortices [18, 19]. The CRVP and horseshoe vortices can be seen in the time averaged flow field, whereas the wake and shear-layer vortices are inherently unsteady features that cannot[18]. The CRVP is the dominant flow structure in the far field of the jet and is thought to be responsible for much of the enhanced mixing and entrainment seen in JICF.

The rich dynamics and wide practical application of the JICF has attracted the attention of numerous researchers [20, 21]. Many previous studies sought to characterize the jet trajectory and mixing rates [15, 16, 22]. The basic scaling for the time averaged trajectory and concentration field of momentum-dominated subsonic nonreacting jets in crossflow is reasonably well understood [16, 23]. However, the trajectory based on the velocity and scalar fields do differ. For example, the trajectory based on the locus of points with maximum velocity penetrates further into the crossflow than the trajectory defined by points of maximum scalar concentration[7, 14]. Most analytically derived correlations for the jet trajectory, based upon either jet velocity or concentration, take the form [21]:

$$\frac{z}{d\sqrt{J}} = A\left(\frac{x}{d\sqrt{J}}\right)^B \tag{1}$$

where J is the momentum flux ratio given by

$$J = \frac{\rho_\mathrm{j} u_\mathrm{j}^2}{\rho_\mathrm{m} u_\mathrm{m}^2} \tag{2}$$

and z is the centerline distance from the wall, d is the jet diameter, ρ_j and ρ_m designate the density of the jet and crossflow, respectively, and x is the distance in the cross-stream direction downstream of the nozzle centerline. The coefficients typically vary between the ranges $1.2 < A < 2.6$ and $0.28 < B < 0.34$, depending upon such parameters as the velocity profile of the jet exit [22, 24], the thickness of the boundary layer [22], and the specific definition used to identify the jet trajectory . Shan and Dimotakis [17] showed that jet trajectory is effectively independent of Reynolds number for transverse jets with Reynolds number in the range $1.0\text{x}10^3 \le Re_d \le 20.0\text{x}10^3$. This paper specifically uses the Holdeman temperature centerline correlation [25, 26], given by:

$$\frac{z}{d\sqrt{J}} = 0.76\left(J^{0.155}\right)\left(\frac{\rho_\mathrm{j}}{\rho_\mathrm{m}}\right)^{0.15}\left(\frac{x}{d\sqrt{J}}\right)^{0.27} \tag{3}$$

for comparison with experimentally observed reacting jet trajectories. This correlation is based upon nonreacting data with momentum flux ratios in the range of $15 \le J \le 60$ and density ratios in the range $0.62 \le \rho_\mathrm{j}/\rho_\mathrm{m} \le 1.0$.

Although not accounted for in the above correlations, the jet injector configuration (e.g. flush-mount or elevated), exit velocity profile, and the crossflow boundary layer profile also significantly affect jet trajectory and dynamics[27]. Elevated injectors exit into the relatively undisturbed crossflow and, therefore jet penetration does not increase proportionally to protrusion distance, due to the greater momentum present in the free stream as opposed to the boundary layer. However, jet elevation also induces co-flow along the length of the injector tube, which acts to promote jet penetration by contributing additional wall-normal momentum to the flow field and shielding the near

field of the transverse jet. The velocity profile at the jet exit also affects the jet trajectory. For example, fully-developed pipe flow carries greater momentum than a top-hat velocity profile with identical mass flow rate, leading to greater jet penetration. Similarly, the crossflow boundary layer thickness influences the jet trajectory because low momentum fluid near the wall effectively increases the jet momentum flux ratio, with a corresponding increase in jet penetration [22].

The jet trajectory is particularly important in reacting flows, as high temperature reaction zones should be located far from combustor walls for durability reasons. Many combustion system performance metrics, such as combustion efficiency, emissions levels, and pattern factor, are also sensitive to jet trajectory. The limited data for reacting jets indicates that the time average jet trajectory is quite close to the nonreacting jet [5, 28, 29]. Hasselbrink and Mungal [29] examined high momentum flux ratio ($J \geq 100$) methane jets issuing from an elevated tube into a low speed wind tunnel. They found that heat release altered the velocity field, but the overall jet trajectory remained quite similar to the nonreacting analogue[29]. Lee and Choi[5] report a similar result in their numerical investigation of $J \approx 20$ fuel jets injected normally into a high-temperature crossflow of diluted air. They found small differences between the cold-flow trajectory correlations and the reacting results, which they attributed to confinement effects [5]. However, there does not appear to be comparable studies for reacting transverse jets at low J where wall interactions may be more significant.

In addition to the trajectory, the location and physical processes controlling flame stabilization are important reacting flow properties. Flame stabilization is a function of such parameters as aerodynamic strain rate, fuel and crossflow chemical composition, crossflow temperature and jet injection geometry. An important distinction in any transverse jet flame stability discussion concerns the jet injector geometry. Elevated injectors, in particular, form bluff-body wake structures that can be important for flame stabilization of low momentum flux ratio jets[30]. Previous studies indicate that flames stabilized on elevated jets can be classified as either lifted or burner-attached [1, 30-32]. The lifted flame regime occurs in higher momentum flux ratio cases where the flame is aerodynamically stabilized away from the burner lip (and the boundary layer) and resembles a lifted axial diffusion flame deflected into the crossflow direction. The burner-attached (or wake-stabilized) regime occurs in low momentum flux ratio cases where jet penetration is insufficient to clearly separate from the burner tube and the bluff-body wake of the jet injector plays a critical role in anchoring the flame [30].

Nominally non-premixed reacting jets in crossflow are often stabilized by a premixed near field [1, 32, 33], at least in lower temperature crossflows. Han and Mungal obtained simultaneous PIV and CH-PLIF measurements that support this claim for an ethylene jet diluted with nitrogen[34] in an 298 K cross flow. They identified a large two-dimensional dilatation zone on the lee side of the jet in the near field that reduced the correlation between the strain rate and CH concentration. This behavior is not seen for non-premixed jet flames in co-flow and suggests that the partially premixed stabilization of transverse jet flames is a result of the interaction of the jet and the crossflow [35]. DNS calculations from Grout et al. [36] on an 420 K hydrogen-nitrogen jet issuing into an 750 K crossflow, showed flame stabilization in a lifted region on the leeward side of the jet approximately 4d from the wall. This area corresponded to both a lower velocity recirculation zone and a point where the mixture was near stoichiometric [36].

Autoignition processes must also be considered with highly preheated crossflows. There are important analogies to the vitiated crossflow problem analyzed here and the Cabra burner, where a non-premixed axial jet flame is stabilized by a high temperature, vitiated co-flow [37-42]. Yoo et al. [42] computed DNS results for a nitrogen-diluted hydrogen jet in an 1100 K co-flow and found convincing evidence of flame stabilization by autoignition, including the presence of HO_2 well upstream of OH containing regions, conditionally-averaged peaks in OH concentration and temperature that shift from lean (i.e. near the most reactive mixture fraction, Z_{MR}[43]) to stoichiometric mixture fractions with downstream distance, and localized regions in the jet near field characterized by low temperature gradients but high reaction rates. Micka and Driscoll considered flame stabilization mechanisms for transverse fuel jets injected into an 1364 K, high velocity air crossflow[44]. Using PLIF imaging, they found an autoignition assisted region on the lee side of the jet characterized by the presence of CH_2O but no OH, CH or CH*. The homogeneous autoignition region appears to anchor a partially premixed flame base and a broken non-premixed flame further downstream.

We next turn to the dynamic features of the reacting JICF. Relatively little is known about the effect of combustion on the transverse jet flow field dynamics, and only recently have researchers made significant progress in understanding nonreacting JICF dynamics [45-48]. Notably, nonreacting JICF at certain conditions exhibit intrinsic, narrowband oscillations characteristic of globally unstable flow fields. For example, iso-density flush-injected jets exhibit a clear bifurcation in their spectral characteristics, which suggests a transition to a globally unstable mode, at velocity ratios less than 3.3 [46]. The same authors find that elevated jets appear to exhibit similar behavior but at lower velocity ratios.

Recent DNS results obtained by Schlatter et al. [47] for a J=9 transverse jet identified two fundamental modes, a high frequency mode found in the shear layer vortices and upright wake vortices, and a lower frequency mode which is strongest in the separated region downstream of the jet. Shear layer vortices are considered the dominant unsteady feature. These structures originate in the high-shear region on the upstream side of the jet and are periodically shed and convected downstream along the mean jet trajectory. Schlatter et al. [47] showed that these shear layer vortices shed continuously with frequency $St=fd/u_j=0.14$ from a one jet diameter long region located in the separated boundary layer upstream of the jet [47]. The upright wake vortices, which link the mean jet trajectory to the flow along the duct wall [49], oscillate with an identical frequency. The second, lower fundamental frequency seen in transverse jets appears most prominently downstream of the jet at St=0.017 and is manifested as a spanwise oscillation [47]. Interestingly, the POD analysis performed by these authors shows that this mode, which is an order of magnitude slower than the SLV modes, has non-zero amplitude everywhere along the jet trajectory, suggesting a global flapping in the spanwise direction, which would have important implications for the reacting case.

The intrinsic, large amplitude oscillations of the transverse jet flow clearly have important implications for fuel/air mixing and unsteady combustion features, such as the propensity of the reacting jet to thermoacoustic oscillations[50]. Recirculation zones in the transverse jet flow field merit particular attention because of their importance in both hydrodynamic stability and flame stabilization. Reversed flow (i.e. backflow) factors prominently in many flow fields exhibiting self-sustained oscillations [51]. On the other hand, recirculating flows also play an integral role in flame stabilization by mixing hot products with cooler reactants, thereby enhancing chemical conversion rates, and providing a suitable low velocity region to anchor a reaction zone. Thus, self-sustained oscillations associated with reverse flow take on special significance in reacting flow fields due to the introduction of fluctuations directly into the flame stabilization zone.

The rest of this paper is organized as follows. The experimental facility and imaging setup are described in Sec.II. Section III.A describes the time averaged trajectories of the flow. Section III.B quantifies the location where reaction initiates and compares these measured locations with calculated autoignition timescales. Section III.C then describes unsteady features of the jet, focusing upon jet flapping behavior, and wrinkle convection. Lastly, section III.D describes unsteady flame-wall interactions.

II. Experimental Facility

This section describes the experimental facility, which is shown in Figure 1. The combustor is situated inside a pressure vessel maintained at 6 atm. It consists of a vitiator, the secondary fuel injector, and the exhaust section. The vitiator air and fuel supply are choked immediately before a 3 m premixing section. The vitiator is supplied with 500 K preheated air and methane and operated at an equivalence ratio of approximately 0.58, in order to maintain an adiabatic flame temperature of 1775 K (calculated) at the burner exit. The vitiator section is a round, 115 mm diameter section. The vitiator terminates into a smooth round-to-square transition, with dimensions of 76 mm x 76 mm, which then flows into the JICF test section. The fuel for the jet was controlled using a separate mass flow regulator and back pressure regulator for each fuel being blended. The cross flow injector, shown in Figure 2, consists of a 20 mm long, 4.3 mm ID tube with a step change to a 17 mm long, 2 mm ID nozzle. The injector protrudes 5mm into the crossflow. Since the injection fuel was not preheated, density calculations are based upon standard values at room temperature. In reality, some conduction of heat back from the hot walls could alter these values. A 76 mm high by 152 mm wide window was used to view the downstream evolution of the reacting jet.

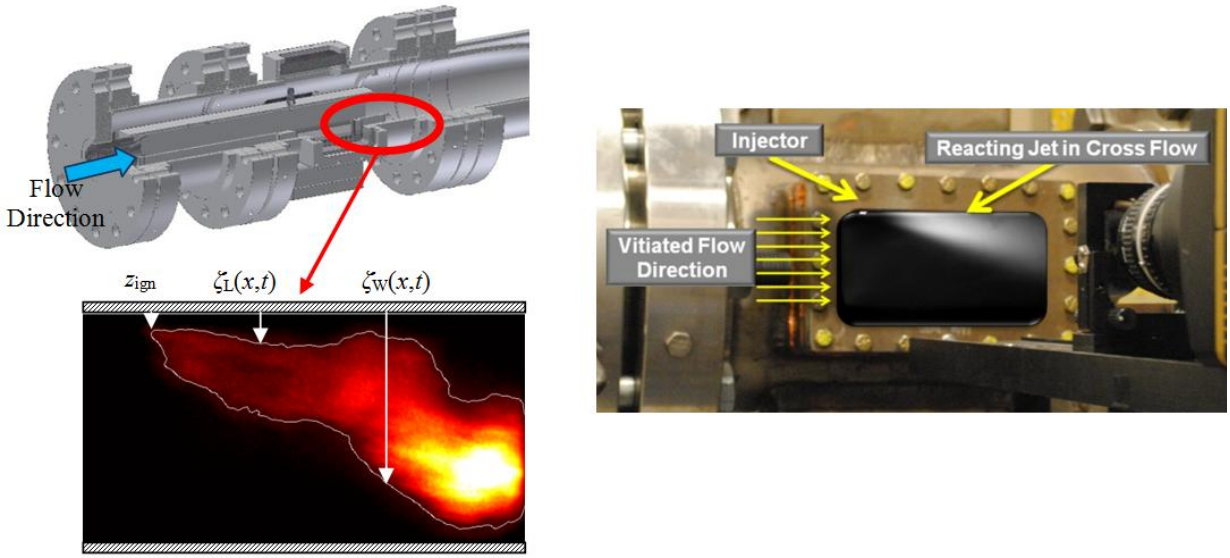

Figure 1. Experimental facility schematic details of injection section (left) and imaging setup (right).

The right image in Figure 1 illustrates this viewing window arrangement and the high speed camera used for visualization. The imaging subsystem consists of a NAC Memrecam GX-3 high-speed camera with a 135 mm f/4 lens, intensifier, and a 430±5 nm filter that allows for imaging of the CH* and CO_2* chemiluminescence from the flame. The line-of-sight, chemiluminescence images were acquired at a rate of 4000 frames per second, with approximately 2000 sequential images obtained at each test point.

Images were obtained with several fuel compositions and momentum flux ratios, *J*, at a nominally constant mean cross flow of 55 m/s. The test conditions are summarized in the table below, along with the calculated temperature rise of the bulk flow due to the secondary reacting jet assuming adiabatic, complete combustion.

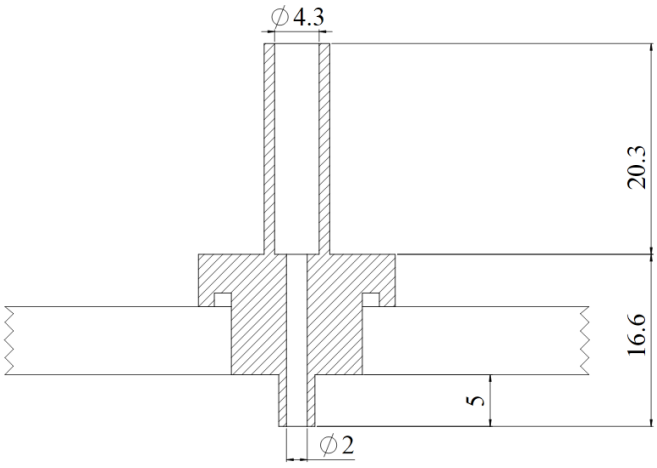

Figure 2. Nozzle cross section with top combustor wall. Dashed lines represent combustor wall. All dimensions in mm.

Table 1: Summary of Test Conditions

Fuel Composition, %			Momentum flux ratio, *J*		Temperature Rise, ΔT [K]	
CH_4	CO	H_2	Min	Max	Min	Max
100	0	0	0.75	35	26	171
50	0	50	5.8	72	60	209
20	0	80	1.3	50	28	165
0	50	50	34	77	54	80
0	30	70	17	240	48	166

III. Results and Discussion

This section presents key results with a discussion first of time averaged quantities, followed by analysis of instantaneous jet dynamics. Specifically, Sec. III.A discusses the time averaged jet trajectory and comparisons with the Holdeman temperature centerline[26]. Sec. III.B then focuses on the time averaged flame initiation point, by quantifying the vertical standoff distance between flame luminosity and the nozzle, z_{ign}, and comparing these results to detailed kinetic calculations of autoignition times. Sec. III.C then analyzes unsteady jet column dynamics and Sec. III.D investigates unsteady flame-wall interactions.

A. Time averaged Jet/Flame Trajectories

Figure 3 shows a typical time-averaged image of the jet in crossflow flame on the left and the imaging setup on the right. Before discussing the jet features, it is important to note the effects of line of sight imaging in interpreting these images. To illustrate, consider the effect of line of sight viewing of a conical flame, as shown in Figure 3. The conical front is a rough approximation for a flame surrounding the fuel jet, which appears to be a reasonable description of the flame downstream of the ignition point. Note the brighter regions at the edges, but also the non-zero brightness in the image center.

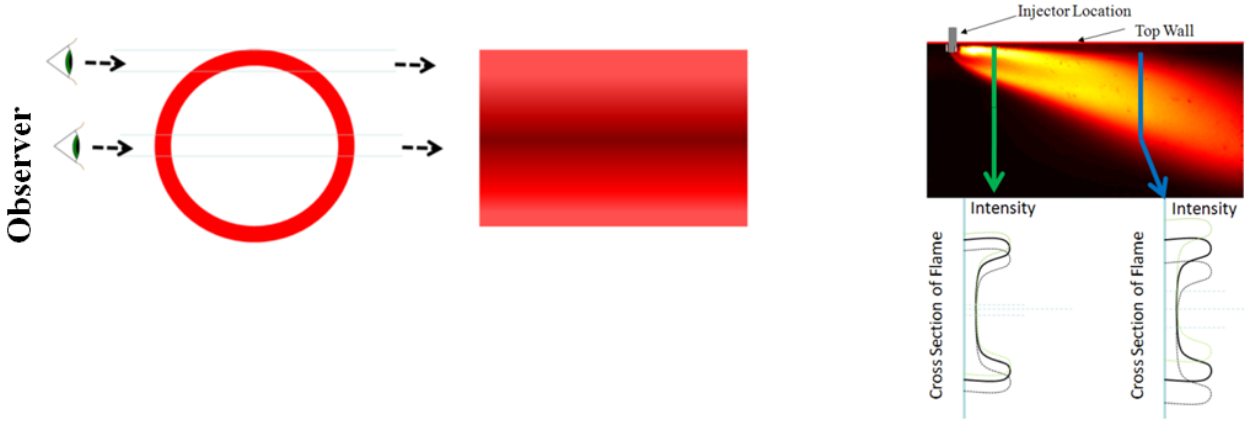

Figure 3. Example of line of sight effects from imaging a cylindrical flame (left) and line of sight effects on images due to vertically moving cylindrical flame (right) . Flame image taken at 50/50 H_2/CH_4, J = 1.3.

The effect of time averaging of the moving flame is illustrated in Figure 3 (a), assuming that the conical flame is moving up and down slightly. Although the image is smeared, it still preserves two local maxima and a local minimum on the centerline. For large displacements, the two maxima are replaced by a single maximum at the centerline. Referring to actual flame data shown in this paper, many of these features can be seen in the images, except very near the jet exit, where more luminosity is evident on the lee side of the jet.

Figure 4 shows intensity averaged chemiluminescence images obtained from CH_4 jet flames for a range of momentum flux ratios, J. The line shows the Holdeman temperature centerline correlation, which quite closely tracks the "dark" middle region of the luminosity image, presumably corresponding to the jet centerline, for approximately the first 30d past the injector center. This result is consistent with other studies showing that the jet trajectory is not substantially altered in cases where the fuel jet is combusting [20, 29]. Farther downstream, the actual reacting jet trajectory clearly penetrates much further into the crossflow for cases with lower momentum flux ratios. The nonreacting correlation remains close to the jet centerline much farther downstream for higher momentum flux ratios. Increased penetration is likely a heat release/dilatation effect whereas reduced penetration is likely a confinement effect.

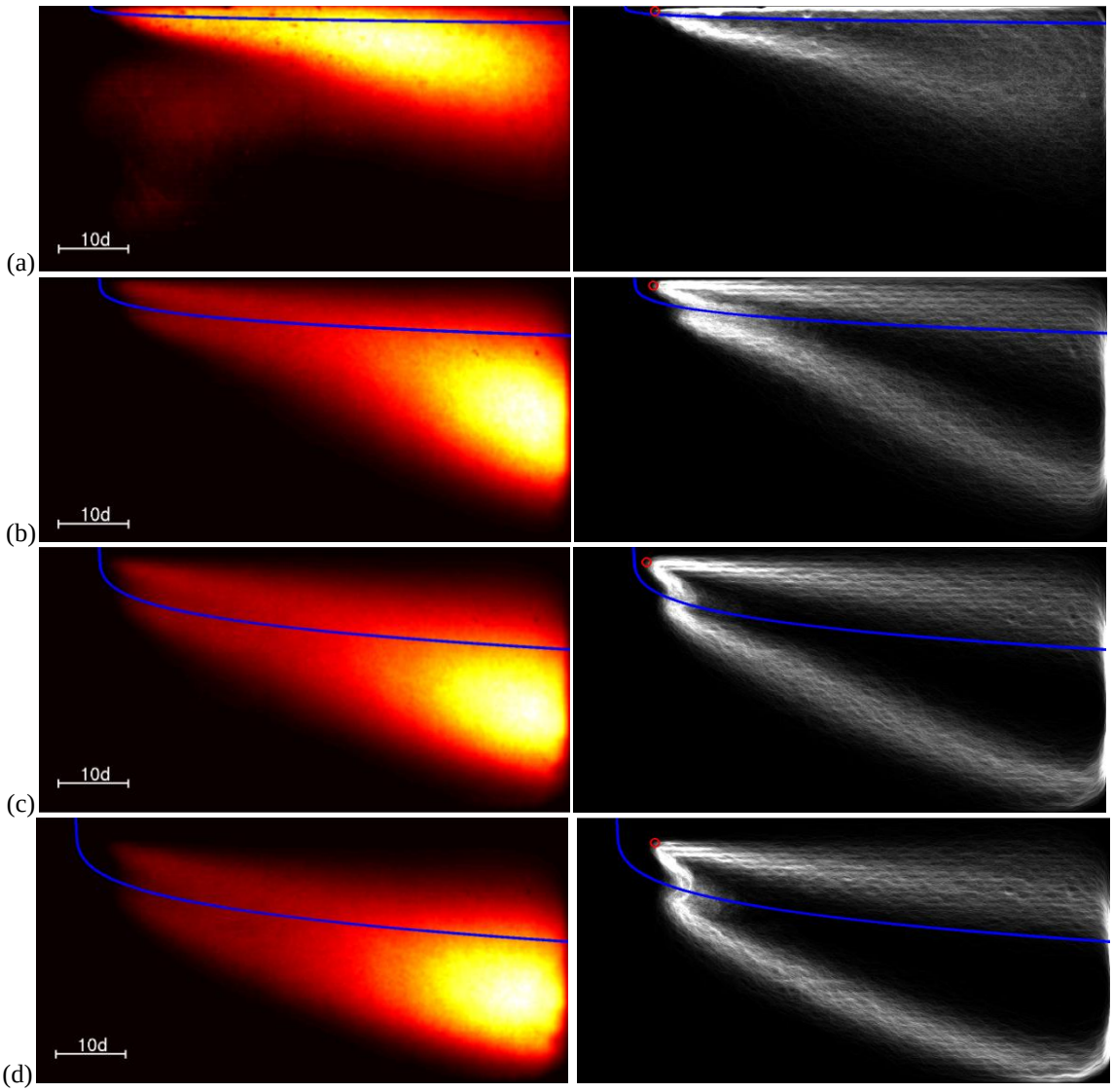

Figure 4. Colorized CH_4 jet chemiluminescence images with overlaid Holdeman temperature centerline correlation (left); average of instantaneous flame edges, with Holdeman temperature centerline correlation (blue), and ignition point (red circle) (right). (a) J=0.75, (b) J=7.2, (c) J=23, (d) J=35.

The instantaneous chemiluminescence images were binarized and an edge tracking algorithm was used to define the coordinates of the leeward, $\zeta_L(x,t)$, and windward, $\zeta_W(x,t)$ edges, defined in Figure 1. The right image in Figure 4 shows an overlay of all flame edges (roughly 2000 images).

Similar results were seen for other fuel compositions in the $1<J<77$ cases. One very high J case was run where the jet clearly penetrated to the opposite combustor wall, as shown in Figure 5. The jet and flame clearly impinges on the lower wall, followed by the luminous flame bending upwards towards the upper wall.

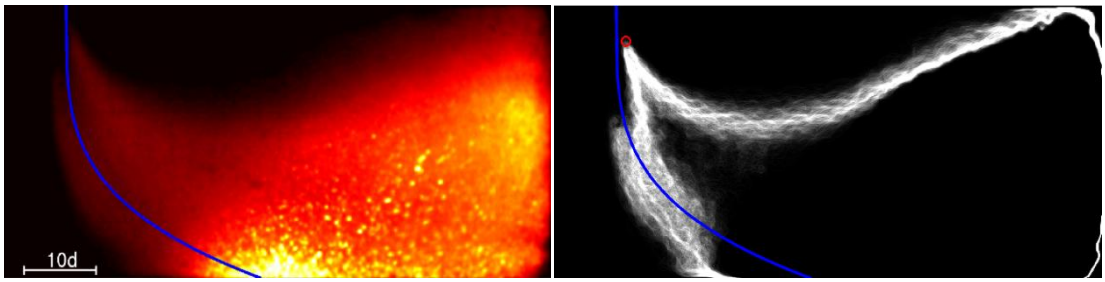

Figure 5. Colorized 70/30 H_2/CO jet chemiluminescence image with overlaid Holdeman temperature centerline correlation (left); average of instantaneous flame edges, with Holdeman temperature centerline correlation (blue), and ignition point (red circle) (right). *J*=240.

B. Time Averaged Flame Initiation Location

This section quantifies the location at which flame luminosity is initiated in the time averaged images. Several representative images showing this ignition standoff are shown in the edge overlay images in Figure 4. For a given momentum flux ratio, the ignition location is heavily dependent on the fuel blend, with pure CH_4 being the furthest from the nozzle, H_2/CO blends usually attached to the nozzle, and CH_4/H_2 blends igniting in a region between the two. Second, the distance between the ignition point and the nozzle is dependent on momentum flux ratio, with higher momentum flux ratios pushing the point of ignition further from the jet. Lastly, the point of ignition always seems to occur on the leeward side of the jet as was seen in studies with cold [29], or preheated [52] crossflow. These points were quantified by extracting the vertical standoff distance between the nozzle outlet and the point of first visible luminosity, z_{ign}.

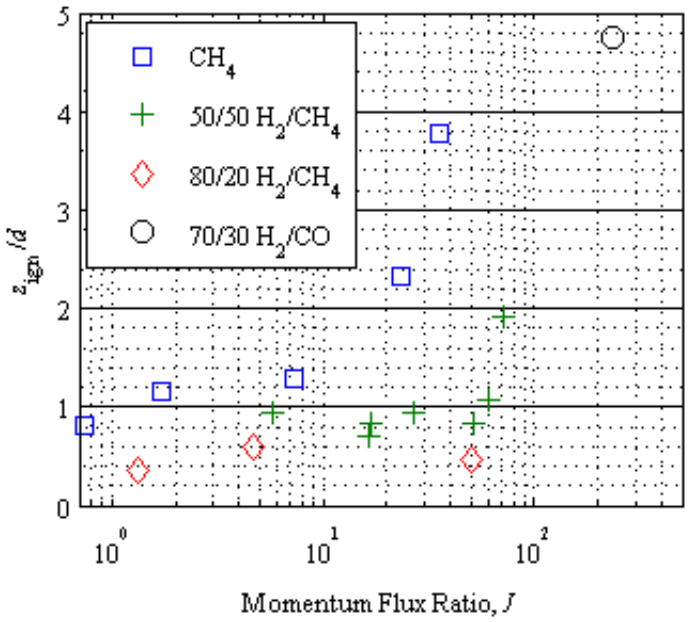

Figure 6. Dependence of normalized vertical flame standoff distance upon momentum flux ratio for methane and hydrogen-methane fuel blends.

Figure 6 plots the dependence of z_{ign}/d upon J for the CH_4, and H_2/CH_4 fuel blends (as noted above, the H_2/CO mixtures are attached to the nozzle with the exception of the single high J case). For reference, one pixel corresponds to z_{ign}/d of 0.12. The best standoff distance estimates are obtained with CH_4, which monotonically increase with J. The vertical standoff distance for hydrogen-methane fuel blends seems to remain relatively constant at 0.5 to 1 nozzle diameters for a range of J, and then increases as this ratio is increased beyond a value of about 60. No clear trends were observed for the horizontal standoff distance, possibly due to the variation in time required to accelerate the jet horizontally between cases of different J.

Further analysis was performed by examining the ratio of the calculated ignition time for the mixture to the measured ignition time where:

$$\tau_1 = \frac{z_{\text{ign}}}{u_{\text{j}}} \tag{4}$$

$$\tau_2 = t_{\text{ign}}\Big|_{Z=Z_{\text{MR}}} \tag{5}$$

The calculated ignition times correspond to the "most reactive" mixture fraction (which is very fuel lean) discussed by Mastorakos[43]. The details of this procedure are given in Appendix I. Figure 7 plots the dependence of the τ_1/τ_2 ratio upon J, showing that it is an O(1) quantity that varies between 1 and 4. We are currently evaluating additional effects not included in this calculation, such as scalar dissipation effects, and the relationship between points of CH* and CO_2* emissions relative to other measures of jet ignition.

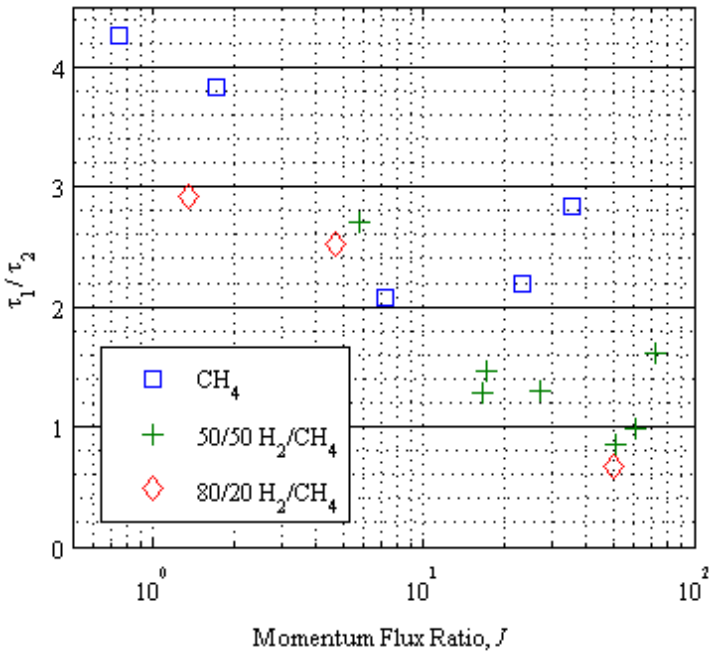

Figure 7. Dependence of measured to calculated ignition time upon momentum flux ratio.

C. Unsteady Flame Characteristics: Jet Column Dynamics

We next discuss unsteady jet features. Figure 8 shows four instantaneous images at the same conditions as Figure 4(c). This image shows that there is considerable jet flapping and downstream convection of wrinkles.

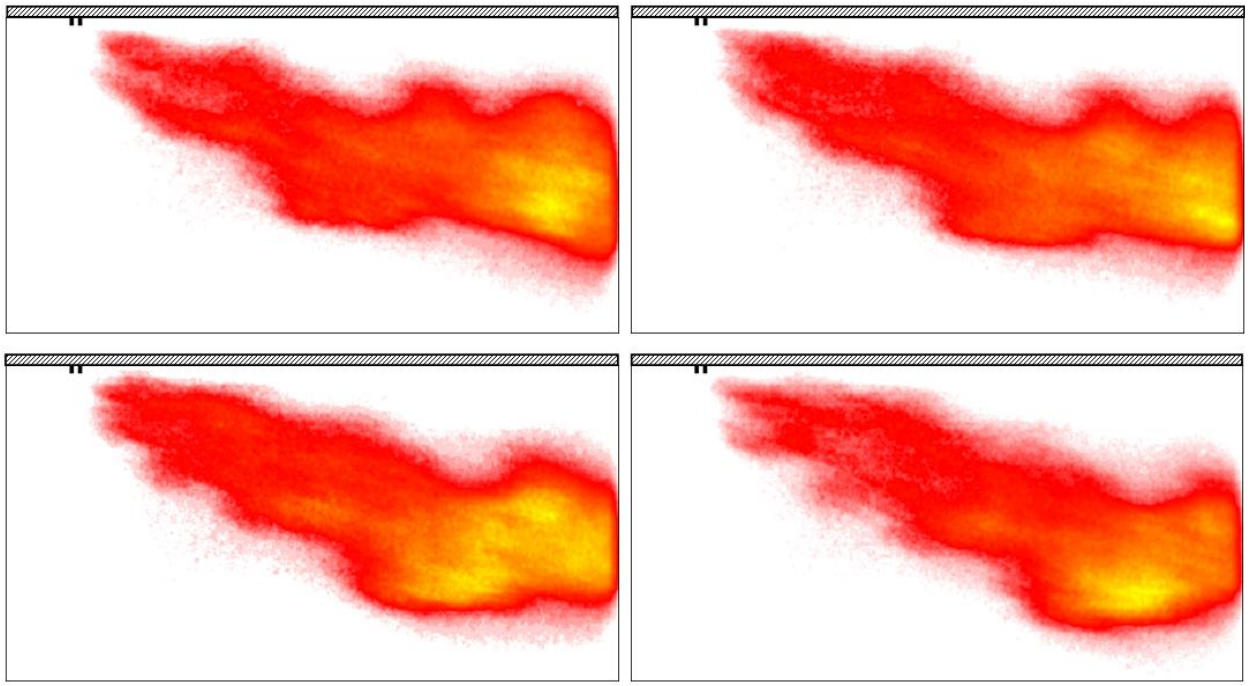

Figure 8. Instantaneous CH* chemiluminescence images for J=23 methane jet.

This large scale flapping motion is sinuous in nature. This was verified by calculating the correlation function between the fluctuations in the top and bottom flame edges as a function of axial location:

$$r^2 = \frac{\left\langle \left(\zeta_W(x,t) - \overline{\zeta_W(x)}\right)\left(\zeta_L(x,t) - \overline{\zeta_L(x)}\right)\right\rangle}{\sqrt{\left\langle \left(\zeta_W(x,t) - \overline{\zeta_W(x)}\right)^2\right\rangle \left\langle \left(\zeta_L(x,t) - \overline{\zeta_L(x)}\right)^2\right\rangle}} \tag{6}$$

These correlation function values were always positive (typically around 0.5). For reference, a near zero value would have indicated no correlation between the top and bottom edges, whereas a negative value would have indicated a varicose, or jet breathing mode. The magnitude of flame flapping can be directly inferred from the width of the jet edge overlays in Figure 4. Jet flapping displacements grow with downstream distance in all cases, as shown in Figure 9, which plots the axial dependence of $\zeta_L^{RMS}(x)/d$. Note also the relative invariance of $\zeta_L^{RMS}(x)/d$ with momentum flux ratio. Note that $\zeta_L^{RMS}(x)$ is given by:

$$\zeta_L^{RMS}(x) = \sqrt{\left\langle \left(\zeta_L(x,t) - \overline{\zeta_L(x)}\right)^2\right\rangle} \tag{7}$$

The downstream convection of the flame wrinkles can be seen by plotting the flame edge position as a function of time and axial position. Figure 10 plots the space-time dependence of the fluctuations in $\zeta_L(x,t)$ normalized by $\zeta_L^{RMS}(x)$, given by:

$$\zeta_L'(x) = \frac{\zeta_L(x,t) - \overline{\zeta_L(x,t)}}{\zeta_L^{RMS}(x)} \tag{8}$$

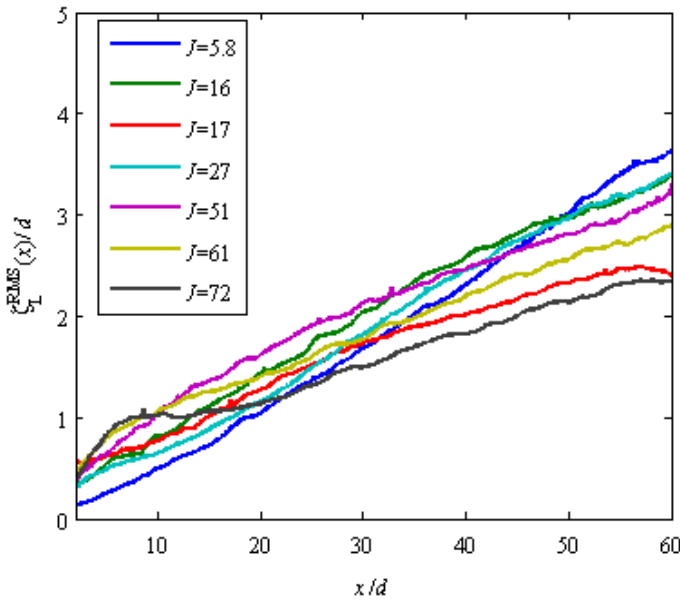

Figure 9. $\zeta_L^{RMS}(x)$ for 50/50 H_2/CH_4 data.

The results clearly show "streaks" corresponding to downstream convection of large and small amplitude fluctuations in flame location. The blue rectangle at the bottom of the image represents the axial location where no luminosity is observed. The top of this rectangle, thus, approximately represents the ignition point. Note that the slope of these streaks can be directly related to the wrinkle convection velocity. Near the ignition point, the velocity appears to be slightly lower for some wrinkles, and increases with downstream distance, suggesting acceleration of wrinkles near the ignition point. For reference, the dashed line denotes the slope of a wrinkle moving at the crossflow velocity of 53 m/s. Note the close correspondence between the slope of the flame wrinkles and the crossflow velocity. For example, estimated convection velocities for the two lines indicated in the figure is 55 m/s in for large x/d. Similar results were obtained for the bottom edge.

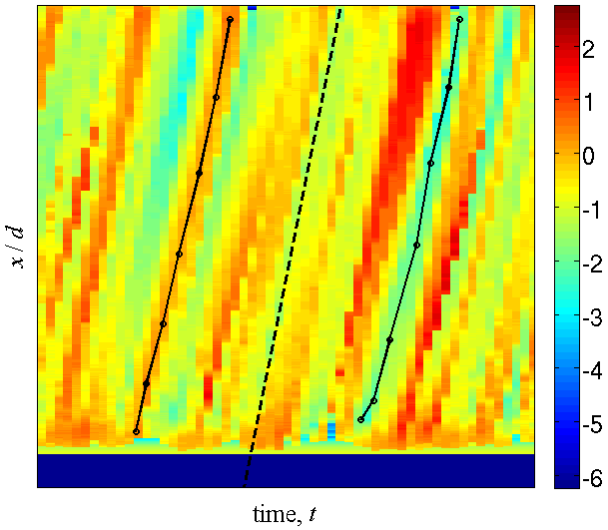

Figure 10. Space-time dependence of $\zeta_L'(x,t)$. Blue indicates edge location closer to bottom wall, whereas red indicates edge location farther from bottom wall. Slope of the streaks represent wrinkle convection velocity. Case shown is J=5.8 50/50 H_2/CH_4.

D. Unsteady Flame Characteristics: Flame-Wall Interactions

In addition to flame dynamics in the interior of the flow, unsteady flame-wall interactions were observed at lower J values. In particular, the jet alternates between being situated very near the upper combustor wall (referred to here as "attached") and then "detaching" into the crossflow. For the lower J values, J<5, there were axial positions where the flame appeared to sit on the wall most of the time, but it would occasionally detach, creating large wrinkles which would convect downstream in the crossflow. Figure 11 illustrates an example of this behavior for a J=1.4 situation.

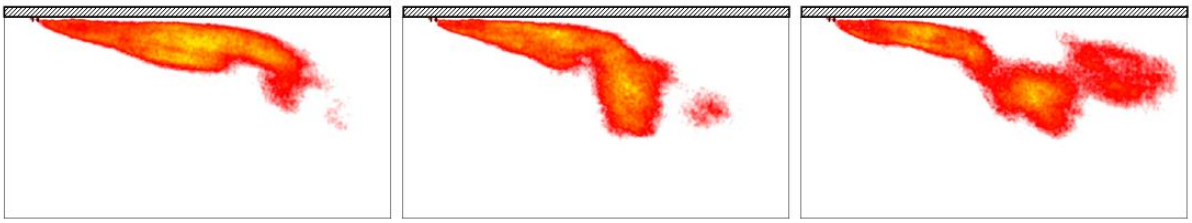

Figure 11. Example of low J jet attachment behavior. Left: jet attached for almost entire length of wall. Middle: jet detached in far field. Right: jet detached closer to nozzle, showing shear layer rollup. All cases are 80/20 H_2/CH_4 at J=1.34.

Interactions of the flame with the upper wall were also observed with larger momentum flux ratios. In these cases, a large scale structure near the nozzle seemed to occasionally cause the flame to attach to the wall. This point of attachment would then convect downstream. Figure 13 shows pictures illustrating this effect for a higher J jet where this behavior was observed.

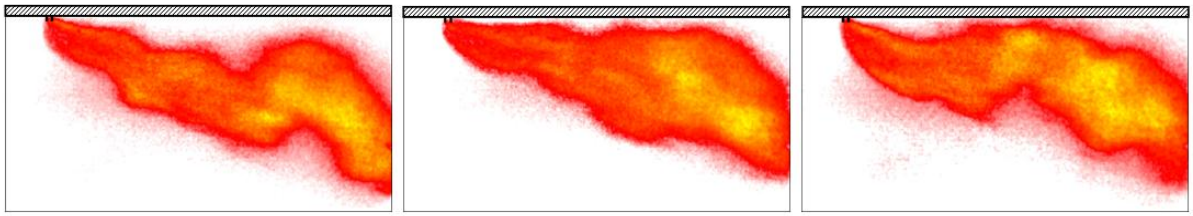

Figure 13. Example of high *J* jet attachment behavior. Left: jet detached from wall. Middle: jet attached in region behind nozzle. Right: jet detached from wall behind nozzle, but attached downstream. All cases are 50/50 H_2/CH_4 at *J*=16.4.

The time varying position of $\zeta_L(x,t)$ is plotted in Figure 12 in order to further illustrate this phenomenon. At low *x/d*, the edge position remained attached to the upper wall (chosen as axial locations less than one jet diameter from the wall and indicated by horizontal green line) for almost all time. For the moderate *x/d* case, one can see behavior where the edge position alternates abruptly from being near the wall to being detached. For the high *x/d* case, the edge position fluctuates substantially as discussed in the prior section, but remains detached for the majority of the time.

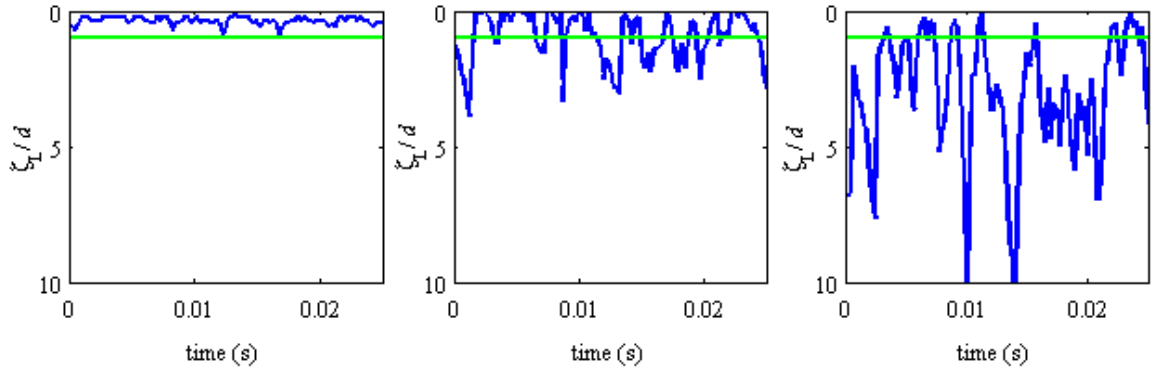

Figure 12. Plot of $\zeta_L(x,t)$ from upper wall vs. time. Blue line is $\zeta_L(x,t)$, and green line denotes one jet diameter. Left: *x/d*=12, middle: *x/d*=29, right: *x/d*=53. Case shown is 50/50 H_2/CH_4, *J*=5.8.

Figure 14 quantifies the fraction of time that methane flames are attached to the wall as a function of axial position, $D(x)$ at several *J* ratios. This duty cycle, *D*, is defined as the amount of time where the leeward edge was within a diameter of the wall divided by the total time:

$$D(x) = \frac{\sum_{t=1}^{n} \left(\zeta_L(x,t) > d \right)}{n} \tag{9}$$

Note the general trend that increasing momentum ratio or axial location leads to a reduction in time that the flame is near the wall. Above a critical *J* value, generally around 20, the flame was rarely near the wall. In addition, some fuel/composition sensitivities at a given *J* value were observed, that likely reflect additional sensitivities to gas expansion ratio across the flame and flame initiation point.

IV. Conclusion

A reacting fuel jet in vitiated crossflow was studied using CH* and CO_2* chemiluminescence imaging and compared with the Holdeman temperature centerline correlation for nonreacting jets in crossflow. Five different fuel blends were investigated: 100% CH_4, 50/50 H_2/CH_4, 80/20 H_2/CH_4, 50/50 H_2/CO, and 30/70 H_2/CO. It was seen that each fuel blend followed the Holdeman temperature centerline correlation in the near field, but deviated in the far field due to expansion effects from heat release. Pure methane and methane-hydrogen fuel blends were found to ignite at an elevated position on the underside of the jet. Varying the jet momentum ratio had little effect on the axial distance between the nozzle and the beginning of the flame; however it had a noticeable effect on the vertical flame

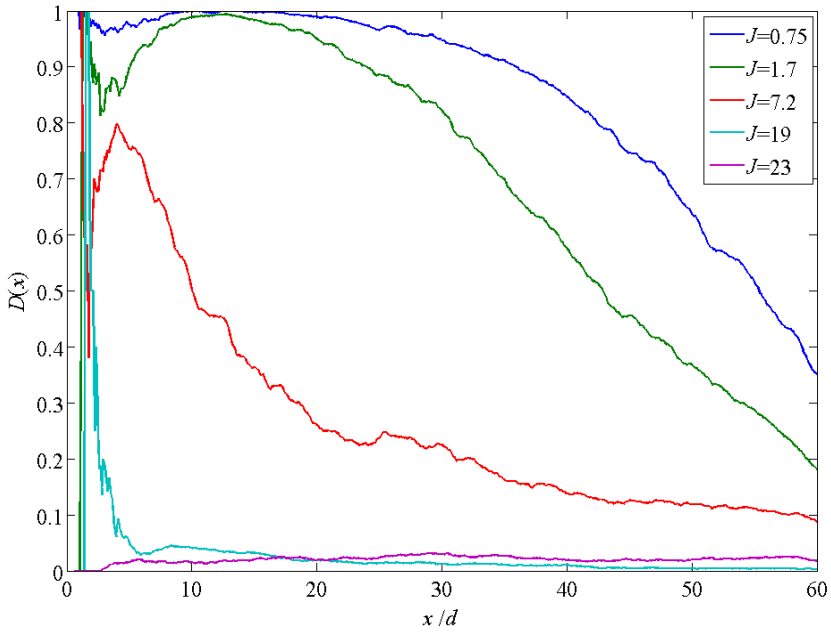

Figure 14. Duty cycle at location *x/d* downstream of injector nozzle for afterinjection for CH_4 cases.

standoff. This distance was found to vary monotonically with momentum flux ratio for pure CH_4, however, for hydrogen-methane blends it remained relatively constant before increasing around a ratio of 60. The vertical standoff distance was converted to a time scale by dividing it by the jet velocity. This time scale was of the same order of magnitude as a chemical time scale calculated as the time for these fuel blends to ignite in a vitiated mixture, and usually varied between 1 and 4 of these chemical time scales. The unsteady motion of the flame edges was examined, which showed a positive correlation coefficient between the top and bottom edges. Furthermore, edge wrinkle convection speeds were found to be ~55 m/s, in agreement with 53 m/s crossflow velocity. Duty cycles representing the fraction of time that the reaction zone was in close proximity to the walls were calculated. It was shown that duty cycle fell off with *x/d* and increasing *J* caused this fall off to happen sooner.

Appendix

This section details the procedure used to calculate autoignition times of unstrained, non-premixed flames using a network of 0-D and 1-D reactors computed with the CHEMKIN software suite. The entire reactor network is treated as adiabatic, and detailed chemistry is computed using the *Chemical-Kinetic Mechanism for Combustion Applications*[53].

A long residence time perfectly stirred reactor (PSR) is used to generate near-equilibrium upstream products approximating those of the vitiator section. Reactants enter the PSR at T=500K. Equivalence ratio is Φ=0.58, and the exit temperature is T=1775K. Next, the hot, vitiated products of the PSR enter a non-reactive gas mixer where they are instantaneously and perfectly mixed with a specified fuel jet gas flow. The fuel jet flow rate and chemical composition vary based on the specific experimental case under consideration. The aggregate mixture enters a 1-D plug flow reactor (PFR) with sufficient length to capture chemical conversion of the jet gas fuels into complete combustion products.

In general, the autoignition delay time is determined by studying the time evolution of a scalar quantity that changes rapidly from the unburnt to burnt state[43]. Autoignition time delay calculations based on maximum gradient conditions extracted from time histories of radical species such as OH or H are commonly found in the literature. In this work, however, autoignition time delay is defined as the time value at which a slug of gas entering the reactor reaches a temperature corresponding to the inlet temperature plus 50% of the total temperature difference between inlet and exit of the PFR. This temperature-based definition alleviates the difficulty of determining autoignition time delays for mixtures with non-zero inlet OH concentration and relatively low total heat release.

The approach outlined above computes autoignition time delay for homogeneous mixtures. In real systems, mixing and chemistry are simultaneous rather than sequential processes in the jet near field, and autoignition phenomena can occur across a range of mixture fractions. Hence a parametric study of autoignition time delay with varying mixture fractions was performed for each fuel jet composition. Representative results are shown in Figure 15.

The ignition time used in the correlations, τ_2, is taken as the minimum ignition time value, which occurs at the "most reactive" mixture fraction, Z_{MR}.

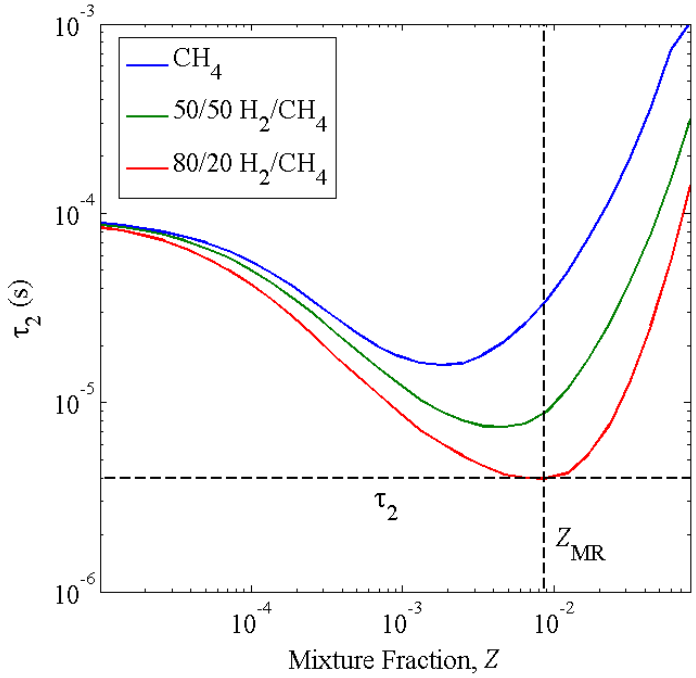

Figure 15. Representative autoignition delay time results for methane/hydrogen blends mixed with lean vitiated product gases at T=1775 K and P=6 atm as a function of mixture fraction. Dotted lines denote Z_{MR} and τ_2 for 80/20 H_2/CH_4 case.

Acknowledgments

The authors gratefully acknowledge Mr. Thomas Shinall, Mr. Andrew Hsu, Mr. Nathan Hadley, and Mr. Robert Adair for their assistance in assembling the experimental facility and data collection.

References

[1]Bandaru, R. V., and Turns, S. R. "Turbulent jet flames in a crossflow: effects of some jet, crossflow, and pilot-flame parameters on emissions," *Combustion and Flame* Vol. 121, No. 1-2, 2000, pp. 137-151.

[2]Boutazakhti, M., Thomson, M. J., and Lightstone, M. "The Effect of Jet Mixing on the Combustion Efficiency of a Hot Fuel-Rich Cross-Flow," *Combustion Science and Technology* Vol. 163, No. 1, 2001, pp. 211-228.

[3]Demayo, T. N., Leong, M. Y., and Samuelsen, G. S. "Assessing Jet-Induced Spatial Mixing in a Rich, Reacting Crossflow," *Journal of Propulsion and Power* Vol. 19, No. 1, 2003, p. 8.

[4]Holdeman, J. D., and Chang, C. T. "The Effects of Air Preheat and Number of Orifices on Flow and Emissions in an RQL Mixing Section," *Journal of Fluids Engineering* Vol. 129, No. 11, 2007, p. 1460.

[5]Lee, K. W., and Choi, D. H. "Numerical study on high-temperature diluted air combustion for the turbulent jet flame in crossflow using an unsteady flamelet model," *International Journal of Heat and Mass Transfer* Vol. 52, No. 25-26, 2009, pp. 5740-5750.

[6]Botros, P. E., and Brzustowski, T. A. "An Experimental and Theoretical Study of the Turbulent Diffusion Flame in Cross-Flow," *Seventh Symposium (International) on Combustion* Vol. 17, No. 1, 1978, pp. 389-398.

[7]Fairweather, M., Jones, W., Lindstedt, R., and Marquis, A. "Predictions of a turbulent reacting jet in a cross-flow," *Combustion and Flame* Vol. 84, No. 3-4, 1991, pp. 361-375.

[8]Lawal, M. S., Fairweather, M., Ingham, D. B., Ma, L., Pourkashanian, M., and Williams, A. "Numerical Study of Emission Characteristics of a Jet Flame in Cross-Flow," *Combustion Science and Technology* Vol. 182, No. 10, 2010, pp. 1491-1510.

[9]Mungal, M., and Lozano, A. "Some observations of a large, burning jet in crossflow," *Experiments in Fluids* Vol. 21, No. 4, 1996, pp. 264-267.

[10]Holdeman, J. D., and Walker, R. E. "Mixing of a Row of Jets with a Confined Crossflow," *AIAA Journal* Vol. 15, No. 3, 1977, pp. 243-249.

[11]Holdeman, J. D., Srinivasan, R., and Berenfeld, A. "Experiments in Dilution Jet Mixing," *AIAA Journal* Vol. 22, No. 10, 1984, pp. 1436-1443.
[12]Leong, M. Y., Samuelsen, G. S., and Holdeman, J. D. "Jet Mixing in a Reacting Cylindrical Crossflow." NASA Technical Memorandum 106975, 1995, pp. 1-31.
[13]Leong, M. Y., Samuelsen, G. S., and Holdeman, J. D. "Mixing of Jet Air with a Fuel-Rich, Reacting Crossflow," *Journal of Propulsion and Power* Vol. 15, No. 5, 1999, pp. 617-622.
[14]Holdeman, J. D., liscinsky, D. S., and Bain, D. B. "Mixing of Multiple jets with a confined subsonic crossflow: Part II - Opposed Rows of Orifices in Rectangular Ducts," *Journal of Engineering for Gas Turbines and Power* Vol. 121, No. 3, 1999, pp. 551-562.
[15]Kamotani, Y., and Greber, I. "Experiments on a turbulent jet in a cross flow," *AIAA Journal* Vol. 10, 1972, pp. 1425-1429.
[16]Broadwell, J. E., and Breidenthal, R. E. "Structure and mixing of a transverse jet in incompressible flow," *Journal of Fluid Mechanics* Vol. 148, 1984, p. 8.
[17]Shan, J. W., and Dimotakis, P. E. "Reynolds-number effects and anisotropy in transverse-jet mixing," *Journal of Fluid Mechanics* Vol. 566, 2006, p. 47.
[18]Fric, T. F., and Roshko, A. "Vortical structure in the wake of a transverse jet," *Journal of Fluid Mechanics* Vol. 279, 1994, p. 47.
[19]Kelso, R. M., Lim, T., and Perry, A. "An experimental study of round jets in cross-flow," *Journal of Fluid Mechanics* Vol. 306, No. 1, 1996, pp. 111-144.
[20]Karagozian, A. R. "Transverse jets and their control," *Progress in Energy and Combustion Science* Vol. 36, No. 5, 2010, pp. 531-553.
[21]Margason, R. J. "Fifty years of jet in cross flow research," *AGARD, Computational and Experimental Assessment of Jets in Cross Flow*. Vol. 1, 1993, p. 41.
[22]Muppidi, S., and Mahesh, K. "Study of trajectories of jets in crossflow using direct numerical simulations," *Journal of Fluid Mechanics* Vol. 530, 2005, pp. 81-100.
[23]Smith, S., and Mungal, M. "Mixing, structure and scaling of the jet in crossflow," *Journal of Fluid Mechanics* Vol. 357, No. 1, 1998, pp. 83-122.
[24]New, T. H., Lim, T. T., and Luo, S. C. "Effects of jet velocity profiles on a round jet in cross-flow," *Experiments in Fluids* Vol. 40, No. 6, 2006, pp. 859-875.
[25]Liscinsky, D. S., True, B., and Holdeman, J. D. "Crossflow Mixing of Noncircular Jets," *Journal of Propulsion and Power* Vol. 12, No. 2, 1996, pp. 225-230.
[26]Holdeman, J. D., Center, L. R., Aeronautics, U. S. N., and Administration, S. *Correlation for temperature profiles in the plane of symmetry downstream of a jet injected normal to a crossflow*: National Aeronautics and Space Administration, 1972.
[27]Moussa, Z. "The near field in the mixing of jet with," *J. Fluid Mech* Vol. 80, No. part 1, 1977, pp. 49-80.
[28]Brzustowski, T., Gollahalli, S., and Sullivan, H. "The turbulent hydrogen diffusion flame in a cross-wind," *Combustion Science and Technology* Vol. 11, No. 1-2, 1975, pp. 29-33.
[29]Hasselbrink Jr, E. F., and Mungal, M. G. "Transverse jets and jet flames. Part 2. Velocity and OH field imaging," *Journal of Fluid Mechanics* Vol. 443, 2001, p. 42.
[30]Huang, R. F., and Chang, J. M. "Coherent structure in a combusting jet in crossflow," *AIAA Journal* Vol. 32, No. 6, 1994, pp. 1120-1125.
[31]Huang, R. F., and Wang, S. M. "Characteristic flow modes of wake-stabilized jet flames in a transverse air stream," *Combustion and Flame* Vol. 117, No. 1-2, 1999, pp. 59-77.
[32]Huang, R. F., and Yang, M. J. "Thermal and concentration fields of burner-attached jet flames in cross flow," *Combustion and Flame* Vol. 105, No. 1-2, 1996, pp. 211-224.
[33]Tsue, M., Kadota, T., and Kono, M. "Detailed measurements of the structure of a jet diffusion flame in a cross flow," *Proceedings of the Combustion Institute* Vol. 28, No. 1, 2000, pp. 295-301.
[34]Han, D., and Mungal, M. G. "Simultaneous measurements of velocity and CH distribution. Part II: deflected jet flames," *Combustion and Flame* Vol. 133, No. 1-2, 2003, pp. 1-17.
[35]Han, D., and Mungal, M. G. "Simultaneous measurements of velocity and CH distributions. Part I: jet flames in co-flow," *Combustion and Flame* Vol. 132, No. 3, 2003, pp. 565-590.
[36]Grout, R. W., Gruber, A., Yoo, C. S., and Chen, J. H. "Direct numerical simulation of flame stabilization downstream of a transverse fuel jet in cross-flow," *Proceedings of the Combustion Institute* Vol. 33, No. 1, 2011, pp. 1629-1637.
[37]Cabra, R., Chen, J., Dibble, R., Karpetis, A., and Barlow, R. "Lifted methane–air jet flames in a vitiated coflow," *Combustion and Flame* Vol. 143, No. 4, 2005, pp. 491-506.
[38]Cabra, R., Myhrvold, T., Chen, J., Dibble, R., Karpetis, A., and Barlow, R. "Simultaneous laser Raman-Rayleigh-LIF measurements and numerical modeling results of a lifted turbulent H2/N2 jet flame in a vitiated coflow," *Proceedings of the Combustion Institute* Vol. 29, No. 2, 2002, pp. 1881-1888.
[39]Gordon, R. L., Masri, A. R., and Mastorakos, E. "Simultaneous Rayleigh temperature, OH- and CH2O-LIF imaging of methane jets in a vitiated coflow," *Combustion and Flame* Vol. 155, No. 1-2, 2008, pp. 181-195.

[40]Gordon, R. L., Masri, A. R., Pope, S. B., and Goldin, G. M. "A numerical study of auto-ignition in turbulent lifted flames issuing into a vitiated co-flow," *Combustion Theory and Modelling* Vol. 11, No. 3, 2007, pp. 351-376.

[41]Wu, Z., Masri, A. R., and Bilger, R. W. "An Experimental Investigation of the Turbulence Structure of a Lifted H2/N2 Jet Flame in a Vitiated Co-Flow," *Flow, Turbulence and Combustion* Vol. 76, No. 1, 2006, pp. 61-81.

[42]Yoo, C. S., Sankaran, R., and Chen, J. H. "Three-dimensional direct numerical simulation of a turbulent lifted hydrogen jet flame in heated coflow: flame stabilization and structure," *Journal of Fluid Mechanics* Vol. 640, 2009, p. 453.

[43]Mastorakos, E. "Ignition of turbulent non-premixed flames," *Progress in Energy and Combustion Science* Vol. 35, No. 1, 2009, pp. 57-97.

[44]Micka, D. J., and Driscoll, J. F. "Stratified jet flames in a heated (1390K) air cross-flow with autoignition," *Combustion and Flame*, 2011.

[45]Bagheri, S., Schlatter, P., Schmid, P. J., and Henningson, D. S. "Global stability of a jet in crossflow," *Journal of Fluid Mechanics* Vol. 624, 2009, p. 33.

[46]Megerian, S., Davitian, J., de B. Alves, L. S., and Karagozian, A. R. "Transverse-jet shear-layer instabilities. Part 1. Experimental studies," *Journal of Fluid Mechanics* Vol. 593, 2007.

[47]Schlatter, P., Bagheri, S., and Henningson, D. S. "Self-sustained global oscillations in a jet in crossflow," *Theoretical and Computational Fluid Dynamics* Vol. 25, No. 1-4, 2011, pp. 129-146.

[48]Davitian, J., Getsinger, D., Hendrickson, C., and Karagozian, A. "Transition to global instability in transverse-jet shear layers," *Journal of Fluid Mechanics* Vol. 661, 2010, pp. 294-315.

[49]Chassaing, P., George, J., Claria, A., and Sananes, F. "Physical characteristics of subsonic jets in a cross-stream," *Journal of Fluid Mechanics* Vol. 62, 1974, p. 25.

[50]Lieuwen, T. C., Yang, V., and Lu, F. K. *Combustion instabilities in gas turbine engines: operational experience, fundamental mechanisms and modeling*: American Institute of Aeronautics and Astronautics, 2005.

[51]Marquillie, M., and Ehrenstein, U. W. E. "On the onset of nonlinear oscillations in a separating boundary-layer flow," *Journal of Fluid Mechanics* Vol. 490, 2003, pp. 169-188.

[52]Kolla, H., Grout, R. W., Gruber, A., and Chen, J. H. "Effect of injection angle on stabilization of a reacting turbulent hydrogen jet in cross-flow," *7th US National Technical Meeting of the Combustion Institute*. Georgia Institute of Technology Atlanta, GA, 2011, p. 7.

[53]"Chemical-Kinetic Mechanisms for Combustion Applications." Combustion Research Group, University of California-San Diego, 2011.